-RESEARCH PAPER-

International Journal of Mining and Geo-Engineering

IJMGE

IJMGE 60-3 (2026) 303-312

DOI: 10.22059/IJMGE.2026.403723.595328

Application of geophysical techniques to identify the causes of roadway instability in conductive ground (Fez region, Morocco)

Brahim Salhi [a,*], Ahmed Benamara [a], Lhoussaine Tarik [b], Khalid Krami [a] Ahmed Hamidi [a] and Mohammed Radouani [a]

[a] *Department of Mechanical and Structural Engineering, National Graduate School of Arts and Crafts, Moulay Ismail University, Meknès, Morocco.*

[b] *Department of Geosciences, Faculty of Sciences and Techniques, Moulay Ismail University, Boutalamine, Errachidia, Morocco.*

Article History:

Received: 20 October 2025.

Revised: 29 January 2026.

Accepted: 08 September 2026.

ABSTRACT

Road instability in marly formations poses a major threat to infrastructure, as water saturation reduces soil-bearing capacity and promotes landslides and subsidence. To address this issue, this study applies an integrated geophysical approach combining electrical resistivity tomography (ERT) and the very low frequency electromagnetic (VLF-EM) method to identify the subsurface causes of pavement failures on three unstable road sections in the Fez-Meknes region (Morocco). Six ERT profiles were acquired along with VLF-EM surveys and subsequently validated by core drilling. The results reveal pronounced conductive anomalies extending to depths of approximately 15–20. These critical anomalies are characterized by very low resistivity values (ρ = 1–5 Ω·m) and interpreted as water-saturated clayey–marly horizons. Moreover, VLF surveys delineate linear conductive zones, while ERT imaging highlights resistivity contrasts and their spatial distribution. Importantly, core drilling confirms that the most conductive zones (< 5 Ω·m) correspond to plastic clayey marls. Thus, this combined ERT–VLF approach enables the identification of vulnerable areas and supports the design of appropriate drainage and stabilization solutions.

Keywords: *Electrical resistivity tomography; VLF-EM; Road instability; Landslides; Marly formations; Pavement creep; Drainage.*

1. Introduction

Road infrastructure built on clay-marl soils is exposed to various forms of instability, including cracking, subsidence, and creep. These problems result in high maintenance costs and can affect user safety. Numerous studies have highlighted the effectiveness of geophysical methods, particularly electrical resistivity tomography (ERT), in detecting and characterizing unstable areas within moisture-associated materials. However, in highly conductive environments, reduced geoelectric contrasts limit the ability to accurately identify unstable areas [1, 2].

Internationally, several studies link road failures to altered clayey or marly horizons, which are often saturated and have low resistivity. In Nigeria, such horizons promote water circulation, progressive loss of bearing capacity, and the appearance of cracks and subsidence [3–5]. In this context, Adesola et al. [3] report low resistivity in degraded sections, generally below 100 Ω·m. This suggests the presence of conductive clayey subgrade. In northern Tunisia, Hamdi Nasr et al. [6] show that landslides develop within saturated clayey-marly formations with very low resistivity. In Egypt, Saad et al. [7] associate the subsidence observed along the Cairo ring road with low- to moderate-resistivity horizons (0.3–200 Ω·m). These are attributed to marly limestone evolving into marly-to-clayey formations, sometimes associated with swelling clays and fractured limestones.

ERT is now widely used for investigating instabilities. It allows the internal organization of the subsoil to be imaged, saturated areas to be identified, and potential failure surfaces to be constrained [8–10]. Recent work also highlights its contribution to delineating the geometry of instabilities, particularly when combined with borehole data [11]. In this context, the Very Low Frequency (VLF-EM) electromagnetic method is an effective tool for rapidly detecting conductive anomalies, such as fractures, altered zones, or discontinuities. These anomalies are frequently associated with areas of increased moisture or water circulation influenced by environmental structure, which reinforces the interpretation of ERT models [12]. Conversely, in conductive environments, the rapid attenuation of ground-penetrating radar (GPR) waves greatly reduces the depth of investigation, limiting exploration to shallow horizons [2, 13].

Refraction seismic also provides additional information about the substrate's mechanical properties [1]. However, it generally remains less sensitive than ERT to water contrasts and plasticized horizons in marls [1, 2, 13, 14]. Despite these limitations, integrated approaches combining several geophysical methods have been proposed in various geotechnical contexts [15–17].

The ERT–VLF coupling remains poorly documented for the analysis of road instabilities in homogeneous and conductive marl formations. The Fez–Meknes region, composed of marl formations with low resistivity and sensitivity to moisture variations, offers favorable conditions for settlement and landslide occurrence. These affect road infrastructure. This study focuses on three road sections in this region that are subject to recurrent instability. Previous investigations, which were mainly geotechnical and isolated, have not clearly identified failure

* Corresponding author. *E-mail address:* b.salhi@umi.ac.ma (I. Salhi).

mechanisms. The main research question is therefore: does the ERT-VLF combination, through integrated analysis, provide a better characterization of the instability mechanisms and delineation of risk areas than conventional geotechnical methods? The objective is to characterize these instabilities using an integrated approach combining ERT and VLF to delineate risk areas, identify the origin of the failures, and evaluate the relevance of this combination as a complement to geotechnical investigations.

2. Study area and observed pavement disorders

2.1. Geological characteristics of the study area

The study area is located in the Fez–Meknes region, along the southern margin of the Pre-Rif domain. This southern sector of the Rifian belt shows significant tectonic deformation. Well-developed folding and faulting are prominent features (Figure 1). The geological substrate consists mainly of marls and clays, which are highly susceptible to water infiltration. This property accounts for the widespread slope instabilities in the region.

Several major fault systems, trending E–W to NW–SE, cut across the area, and a dense network of secondary fractures also exists. These structural discontinuities govern groundwater circulation by providing pathways for infiltration and subsurface flow. In addition, they strongly control surface drainage. As a result, the area's dendritic drainage pattern reveals the low permeability of the marly formations, as runoff tends to concentrate along fractures and other weak zones.

Marly formations have low intrinsic permeability. This favors the gradual buildup of water in the soil mass. Over time, this process degrades the soil's mechanical properties and increases its tendency to deform. During intense or prolonged rainfall, saturation becomes more severe. This greatly raises the likelihood of settlement and landslides.

2.2. Pavement disorders observed in the study area

Damage has been observed over a very long section of the roads studied (Figure 2). The geological characteristics of the existing terrain have caused a very specific landslide on the left side of the road P5007 (towards My Yaacoub), which is also marked by very frequent advanced cracking (Figure 2a). Rotational breaks (Figure 2b), punching (Figure 2c), landslides and cracking (Figure 2e), as well as damage to concrete drainage ditches (Figure 2e) have been identified. The My Yaacoub site has undergone multiple maintenance interventions due to recurring problems. Faced with the progressive deterioration of the initial route despite successive reinforcements, the administration decided to divert it towards the ridge. The objective of this geophysical study is to identify the underground causes of these instabilities and to validate the new route.

The second site (My Idriss) is on the N13 national road, a few kilometers from Meknes toward My Idriss Zerhoun. It shows repeated damage, such as subsidence and surface slippage (creep, Figure 3).

The third site (N6, south exit of Meknes) mainly has drainage problems. The three road sections in question are located at three separate sites. The location and coordinates of the areas studied are shown in Table 1.

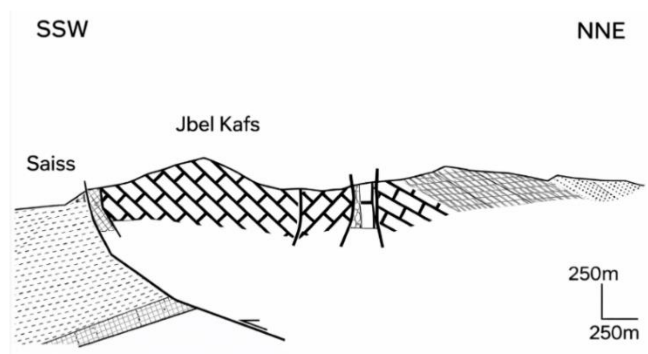

Figure 1. SSW-NNE geological cross-section of the folded-faulted structure of the South Rifian Ridges (after Fangères, 1987; modified by Benmakhlouf [27]).

Table 1. Location of the investigated road sections.

Site	Road	Location
My Yaacoub	P5007	X=34,0811 Y=5,1705 Z=352,7 m
My Idriss	N13	X= 484250,376 Y=371818,732 Z= 500 m
N6 sortie sud de Meknès	N6	X=488046, 313, Y=360732,802 Z=620 m

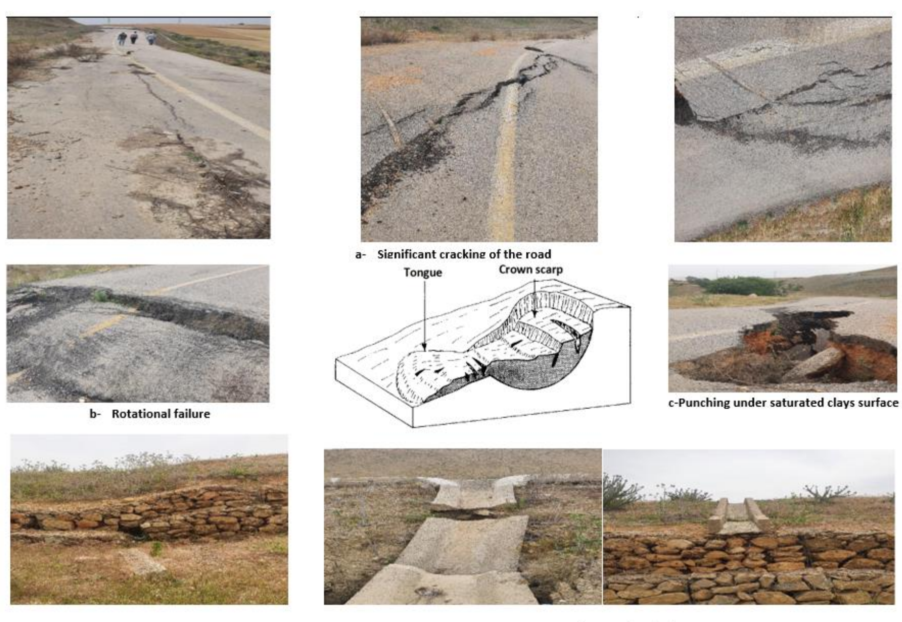

Figure 2. Road subsidence and cracking on the My Yaacoub section (P5007 road).

Figure 3. Pavement creep observed at the My Idriss site (N13 road).

3. Materials and methods

3.1. VLF-EM and ERT methods

To study road instability at the three sites, two complementary geophysical methods were employed: very low frequency electromagnetic tomography (VLF-EM) and electrical resistivity tomography (ERT). VLF-EM uses very low-frequency radio waves, based primarily on a simplified form of Maxwell's equations, to rapidly identify conductive anomalies associated with fractures and altered zones where water flows, making it particularly well suited for reconnaissance surveys. ERT, on the other hand, generates subsurface images that highlight lithological variations and delineate the extent of saturation. VLF-EM provides rapid spatial coverage, while ERT offers greater accuracy and detail. Combined, these methods allow for extensive coverage and high-resolution subsurface characterization.

The methodology followed a two-step process. In the first stage, VLF-EM profiles were acquired along each road segment using a T-VLF receiver (IRIS Instruments, Orléans, France). Measurements were taken at regular intervals (10 m increments) to ensure continuous coverage. The data were processed using Fraser and Karous-Hjelt filtering, which highlighted linear structures interpreted as active flow paths and emphasized potentially problematic areas. Based on insights from this initial step, the workflow transitioned to detailed ERT surveys, as described below.

After preliminary analysis of the VLF profiles, detailed electrical resistivity surveys (ERTs) were conducted with an ABEM Terrameter LS 2. Survey lines were positioned based on surface observations and VLF-EM anomalies. This approach made deployment of the time-consuming resistivity measurements more efficient. The acquired data were inverted using the Res2DInv software [26]. The depth of investigation (DOI) index was calculated to assess model reliability.

The integration of these data facilitated mapping wetlands, disturbed areas, and fracture channels that channel water toward the pavement, thereby enabling the identification of weak points at the three sites.

3.2. Depth of investigation (DOI) assessment

To determine whether the characteristics of the 2D imaging results are due to the data or to artifacts related to the inversion process, we performed a sensitivity test. It was calculated the Depth of Investigation (DOI) index [16] for this purpose. This index assesses the depth beyond which the inversion is no longer sensitive to the subsurface's physical parameters. The DOI calculation involves two inversions on the same dataset. Each inversion starts from a symmetrically perturbed reference model: one with resistivity 0.1 times the initial model and another with resistivity 10 times the initial model. Factor αs determines the extent to which the reference model affects the inversion. It is set to 0.01 times the smoothing factors, which are set to 1. Another essential parameter for calculating the DOI is the depth of the inversion mesh. This area must be large enough to cover where reliability is compromised. It was chosen a mesh depth equal to three times the maximum investigation depth estimated for the measurement device [13, 16, 23]. The DOI value is given by the equation [16].

$$R(x,z) = \left|\frac{m_1(x,z) - m_2(x,z)}{(m_{1r} - m_{2r})}\right| \quad (1)$$

Here, m_{1r} and m_{2r} denote two different reference models, $m_1(x,z)$ and $m_2(x,z)$ represent the inverted resistivity obtained from these reference models, and $R(x,z)$ is the DOI index for a given model cell. To reduce the influence of the damping factor (which limits large model changes) and the choice of starting models, we normalized the DOI. The equation was used from [24]:

$$R(x,z) = \left|\frac{m_1(x,z) - m_2(x,z)}{R_{max}(m_{1r} - m_{2r})}\right| \quad (2)$$

where R_{max} is the maximum value of R.

A DOI close to 0 indicates areas where the model is highly dependent on the data. Conversely, this index tends toward 1 in areas under the reference models' control. The main challenge is to define a threshold for reliable resistivity values. For example, Marescot et al. [13] recommend 0.1 or 0.2. In this study, a DOI of 0.2 was used. The curves representing this threshold are superimposed on the inverted sections of the different ERT profiles. These profiles were obtained in the study areas. Generally, the chosen threshold matches the maximum depth obtained by the different electrical resistivity models for the three sites studied.

3.3. ERT inversion quality control (absolute error)

The quality of the ERT models was assessed based on the Abs. error (%) reported by the inversion software, corresponding to the average misfit between the measured apparent resistivity and those recalculated from the inverted model [25, 26]. The values obtained for all profiles are summarized in Table 2 and range from 1.48% to 17.3%. With the exception of the ERT1 profile at My Yaacoub (17.3%), the errors remain low (≤ 4.9%), indicating good acquisition quality and an overall stable inversion. The highest error on ERT1 at My Yaacoub may be due to a more heterogeneous, human-modified environment, which could increase the fitting error. These indicators are presented here as quality control measures. The detailed geological interpretation is developed in the "Results and Discussion" section.

4. Results and discussion

4.1. My Yaacoub site

At the My Yaacoub site, two VLF profiles (P1: 250 m along the abandoned road section; P2: 100 m on the downslope embankment) and two ERT profiles (ERT1: 310 m along the abandoned section; ERT2: 155 m along the new alignment) were acquired (Figure 4).

The VLF P1 profile shows a generally homogeneous response, with no significant electromagnetic anomalies. A minor, shallow, and localized signature is observed near 100 m (Figure 5). The VLF P2 profile (Figure 6). processed using Karous–Hjelt filtering, identifies a distinct anomaly characterized by a negative real component and concentrated equivalent current density, centered at X = 25 m with an apparent vertical extent of approximately 8–20 m. Field observations confirm the installation of a road embankment to mitigate recurring landslides.

In the abandoned road section, ERT1 (Figure 7a) indicates a predominantly conductive environment (approximately 1–5 Ω·m), which likely reflects saturated marl-clay horizons overlain by moderately resistive layers (approximately 15–36 Ω·m) associated with disturbed or altered materials. Two deep resistive structures are identified.

Table 2. Inversion errors of the ERT profiles (Abs. error, %).

Site	ERT Profile	Profile length (m)	Inversion error (%)	Inversion quality
My Yaacoub	ERT 1	310	17,3	Moderate
My Yaacoub	ERT 2	155	1,48	Excellent
My Idriss	ERT	155	4,9	Very good
RN6	ERT 1	155	1,69	Excellent
RN6	ERT 2	155	1,57	Excellent
RN6	ERT 3	155	3,6	Very good

Figure 4. Aerial view of the My Yaacoub site showing the original road layout and VLF-ERT geophysical profile locations.

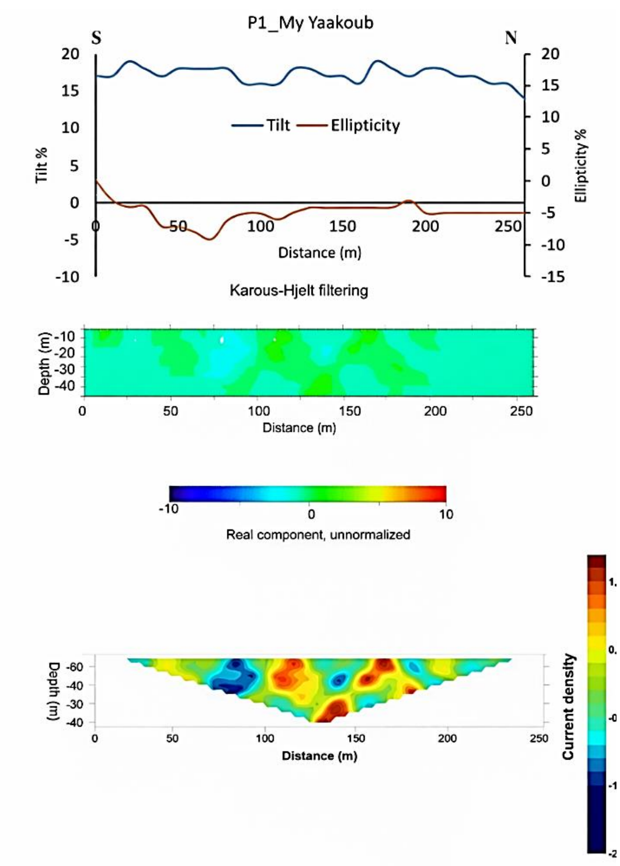

Figure 5. VLF profile P1 My Yaacoub: Tilt and Ellipticity, Karous-Hjelt filtering, current density (10 m spacing, S-N direction).

The first anomaly, located between X = 130–160 m, is interpreted as a more compact, mechanically resistant domain composed of denser, less saturated materials, potentially related to bedrock relief or a coarser unit. Spatial correlation with the VLF anomaly (X = 25 m) suggests a structural contact between a resistant domain at depth and reworked, moist materials at the surface. The second anomaly, centered near 220 m, extends laterally for approximately 50 m, is situated between 20 and 40 m depth (maximum approximately 30 m), and is associated with resistivity of 35–80 Ω·m. This structure is also interpreted as a compact, mechanically resistant domain, likely corresponding to a coarser, less saturated relief.

Along the new road alignment, the Wenner and dipole-dipole configurations detect a shallow conductive anomaly at X = 105, attributed to moist clayey materials or heterogeneous backfill. The apparent thickness is greater in the Wenner configuration (Figure 7b) (approximately 4 m) than in the dipole-dipole (Figure 7c) configuration (approximately 2.5 m), reflecting the differing sensitivities of these devices. These findings suggest that saturated fine materials, in combination with localized structural heterogeneities, significantly contribute to instability. Nevertheless, the geometry and depth of any potential failure surface require further targeted geotechnical calibration.

A synthesis of the ERT profile results, including the locations, depths, resistivity ranges, and interpretations of the main geophysical anomalies, is presented in Table 3.

In summary, the geophysical findings indicate that moisture and structural heterogeneities are key to the site's instability. Highly conductive zones (≈1–5 Ω·m) reveal saturated marly-clayey horizons with poor hydrogeological conditions. These include high moisture and clay content, which reduce the subgrade's strength. The realigned route shows an overall more favorable configuration: only a single conductive anomaly is identified, well constrained spatially, with a lateral extent of about 20 m and a maximum depth of about 4–5 m in the most unfavorable case (Wenner configuration). These results support realigning the route. Effective and durable drainage measures are needed for the new segment.

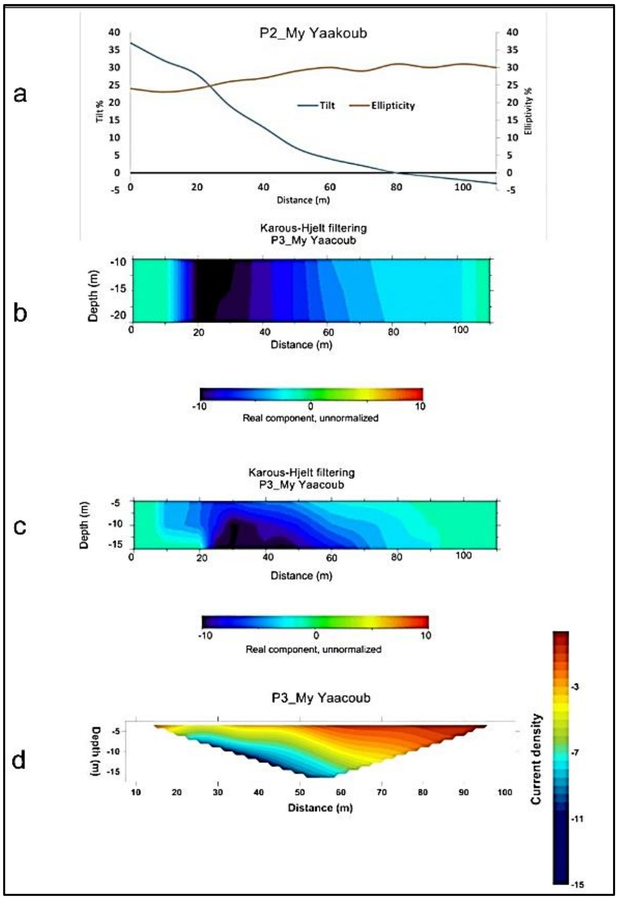

Figure 6. VLF Profile P2 My Yaacoub : (a) Tilt et Ellipticity, (b) Karous-Hjelt filtering (10 m spacing), (c) Karous-Hjelt filtering (5 m spacing), (d) Current density.

To validate these geoelectrical interpretations, core borehole S9, drilled near the ERT1 profile as part of a geotechnical investigation, was used as a lithological reference. The exact horizontal distance between the borehole and the profile axis cannot be determined because the source document lacks planimetric coordinates. However, the borehole was drilled directly on the old road platform, making it particularly useful for assessing the alignment between geophysical results and actual subsurface conditions.

The lithological sequence in S9 (Table 4) is mostly marly, changing from yellow-brown at the surface to blue-gray at depth. Scattered gypsum layers and sandier zones near the top likely represent reworked road fill. This stratigraphy closely aligns with the ERT model. Higher surface resistivity (around 15–35 Ω·m) is found in the upper 3 m, indicating disturbed, coarser material, while lower resistivity (0.2–6 Ω·m) corresponds to finer, marly beds between 3 and 15 m depth, consistent with blue-gray marls below 8 m in S9. The ERT section shows more gradual interfaces than the borehole log due to ERT's volumetric averaging and limited resolution. These detailed layer-to-layer correlations validate the geoelectrical interpretation by clarifying how each lithological feature matches the geophysical response.

4.2. My idriss site

The second site, designated My Idriss, is located on National Route 13, between Meknes and My Idriss Zerhoun, in Ouled Ncir. At this location, two very low frequency (VLF) profiles and one electrical resistivity tomography (ERT) profile were acquired (Figure 8).

The VLF measurements indicate a predominantly homogeneous environment along the route. However, profile P1 (Figure 9 exhibits a distinct electromagnetic anomaly, centered at approximately x = 125 m. This anomaly is consistently observed on the Tilt/Ellipticity curves, the Fraser profile, and the Karous-Hjelt pseudo-section (Figure 9). In contrast, profile P2 (Figure 9) shows a moderate anomaly at the beginning of the route, around x = 20 m. This suggests a surface variation in the infill materials and underlying fine deposits.

The ERT profile (Figure 10) reveals critical subsoil conditions. The surface layer shows high resistivity (20–70 Ω·m, locally 140 Ω·m), reflecting road fill materials. Between 25 and 70 m, a thick resistive zone (about 6 m) represents embankment and pavement reinforcement, intended to reduce settlement due to creep observed at the site. Near the beginning (0–10 m), a shallow conductive zone (2–10 Ω·m) marks moist clayey-marl materials.

Below this layer, in the highly resistive reconstruction zone (25 to 70 m), lies a deep and highly conductive layer ($\rho < 5$ Ω·m) approximately 10 m thick. This zone contains water-saturated clay-marl horizons and is likely responsible for the observed pavement creep. The spatial correlation between the deepest and thickest conductive zone (10–20 m below the 25–70 m section) and the thickest surface reconstruction layer (approximately 6 m) confirms that the most significant subsidence occurred where subsurface saturation is most pronounced.

Although the two profiles differ in length (VLF: approximately 300 m; ERT: approximately 155 m), they were both positioned to target the same central zone, with a low positioning uncertainty (approximately 2–4 m). The pronounced vertical conductive anomaly observed on the ERT profile, near x = 20–70 m, corresponds to the P1 anomaly of the VLF profile (x = 100–150 m) (Figure 9), although the positions are slightly different due to the difference in profile scale. This correlation suggests that both methods likely detect the same structural discontinuity or preferential water-infiltration pathway, thereby intensifying the saturation of the underlying clay horizons.

To validate the geophysical interpretation, the OH4 core borehole was drilled at the My Idriss site. The observed lithological succession is presented in Table 5. The OH4 borehole (0–10 m) reveals a marl-dominated sequence. A layer of calcareous sandstone located between 3.7 and 6.0 m interrupts this. This stratigraphic organization is consistent with the electrical resistivity tomography (ERT) profile. The marl layers correspond to deep conductive zones (approximately 2–5 Ω·m). The calcareous sandstone layer corresponds to the moderate-resistivity zone observed at intermediate depths. Thus, borehole OH4 provides direct lithological confirmation of the marl-dominated stratigraphy which is responsible for the site's instability.

At site 2, pavement treatment must be integrated with optimized infiltration water management. Geogrid reinforcement increases load-bearing capacity and reduces progressive deformation, as demonstrated by case studies in similar geological contexts. Effective drainage of the pavement platform, combined with targeted deep drainage using subhorizontal drains at the structural contact, reduces the water content of the clay formations and limits their creep.

4.3. RN6 (southern Meknes) site

The final road section in our study is located on National Route 6 (Fez–Rabat), just south of Meknes, in a predominantly clayey area. Measurements were taken near a plaster factory (Inno Plâtre, Figure 12). Within this geological context, geophysical investigations were conducted to identify the source of the water observed in the unlined drainage ditches during the rainy season which affected approximately 50 m of the road.

Three electrical resistivity tomography (ERT) profiles (Figure 12) were acquired parallel to the roadway: ERT1 and ERT2, on either side of the road, approximately 24 m apart laterally, and ERT3, approximately 150 m south of the section, with a slightly oblique orientation. It should be noted that ERT3 is far from the ditches; it was conducted on an unpaved street between the factories. In addition, two very low frequency (VLF) profiles were acquired. P1_RN6 shares the same central point as ERT1, although their lengths differ (ERT1: 155 m; P1_RN6: 200 m), while P2_RN6 is co-located with the ERT3 profile. The objective is to identify preferential infiltration zones. The correlation between the VLF and ERT data is generally consistent. On the P1 profile (Figure 13), the VLF signal (P1_RN6, x = 90–130 m) corresponds to a

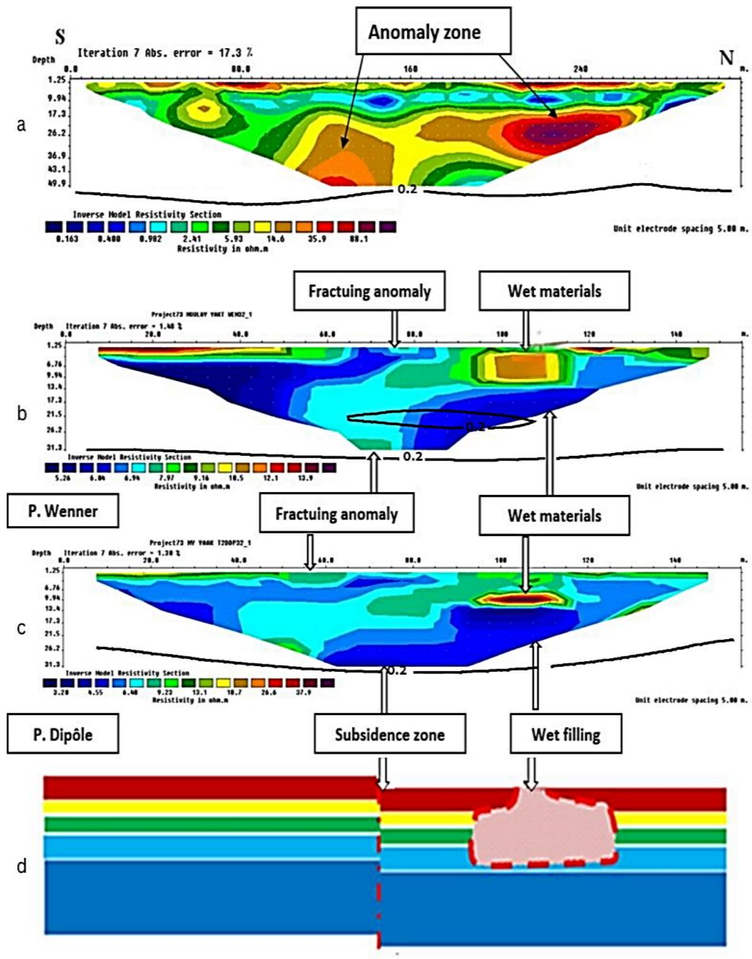

Figure 7. ERT profiles My Yaacoub: (a) Abandoned road section, (b-c) new road section (Wenner and dipole-dipole arrays). DOI = 0.2 threshold line and interpreted structural contact shown.

Table 3. Summary of the main ERT anomalies and proposed interpretation (My Yaacoub site).

Profile	Chainage (m)	Depth below surface (m)	Resistivity	Interpretation
ERT-1	0–310	0–1.5	15–36 Ω·m	Disturbed surface fill / altered materials
ERT-1	0–310	≈1.5–15	0.2–6 Ω·m	Saturated marly–clayey horizons
ERT-1	≈130–160	≈20–40	>15 Ω·m (locally >35)	Compacted and resistant domain (denser, less saturated materials)
ERT-2 (Wenner)	≈95–115	0–5	10 – 13 Ω·m	Humid clayey materials / reworked fill
ERT-2 (Dipole–dipole)	≈95–115	2,5–5	25–38 Ω·m	Same anomaly, thinner apparent thickness

Table 4. Lithological log of borehole S9 (My Yaacoub).

Depth Interval (m)	Thickness (m)	Synthetic Lithology
0.0 – 0.5	0.5	Topsoil/vegetation layer
0.5 – 3.0	2.5	Altered sandy yellow-brown marl
3.0 – 8.0	5.0	Yellow-gray marl (sandy to semi-indurated, locally gypseous)
8.0 – 17.0	9.0	Gray-yellow semi-indurated marl (gypsum lenses)
17.0 – 23.0	6.0	Blue-gray indurated sandy marl

Table 5. Lithological log of borehole OH4 (My Idriss).

Depth Interval (m)	Thickness (m)	Synthetic Lithology
0.00 – 1.80	1.80	Topsoil/vegetation layer
1.80 – 3.70	1.90	Yellow-greenish marl
3.70 – 6.00	2.30	Calcareous sandstone
6.00 – 10.00	4.00	Yellow marl

Figure 8. Aerial view of the My Idriss site showing VLF-ERT geophysical profile locations.

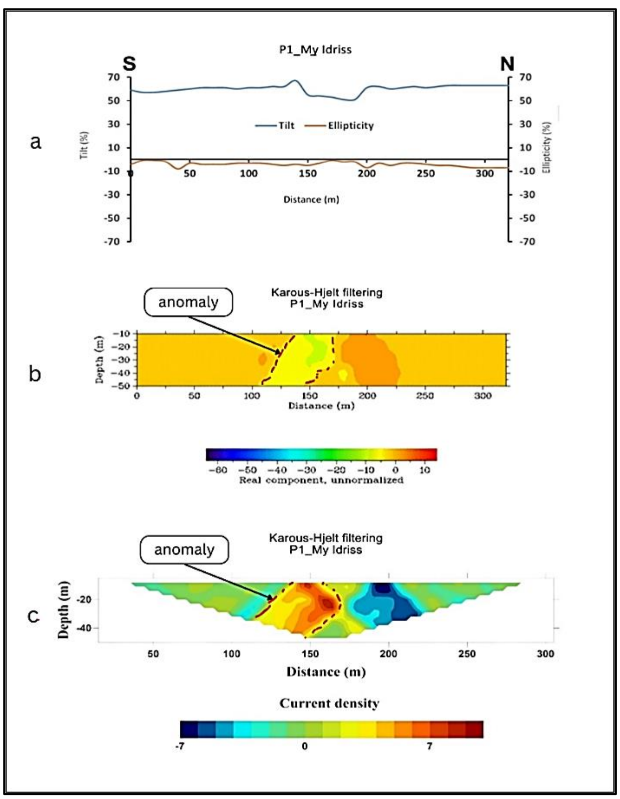

Figure 9. VLF profile My Idriss P1: (a) Tilt and Ellipticity, (b) Karous-Hjelt filtering (10 m spacing), (c) Current density.

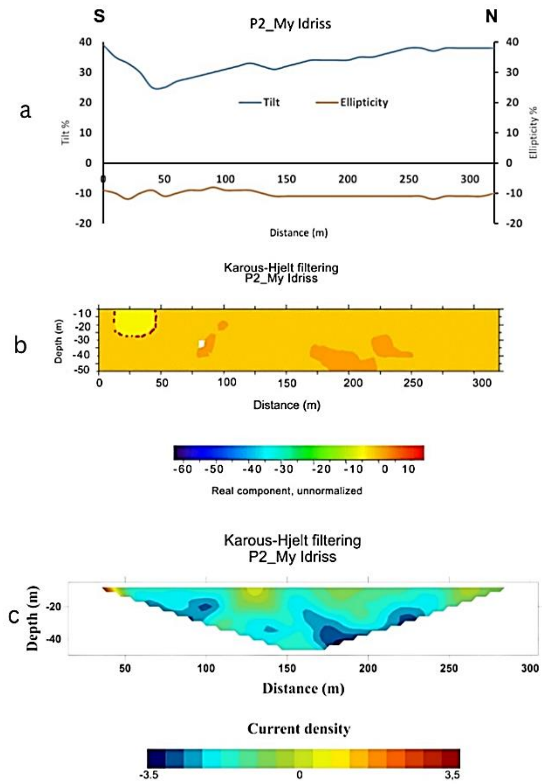

Figure 10. VLF profile My Idriss P1: (a) Tilt and Ellipticity, (b) Karous-Hjelt filtering (10 m spacing), (c) Current density.

zone of low resistance visible on the ERT1 profile (resistance ≈ 10–50 Ω·m, x ≈ 70–105 m). This confirms the presence of a more conductive area, likely related to damp soil or sections with water-heavy clay or marl. The nearby profile ERT2, though offset by about 24 meters, also finds a conductive area in about the same place. This shows the issue spans the entire width of the road.

In addition to the findings on the ERT1 and ERT2 profiles, ERT1 also reveals, between approximately 0 and 35 m, surface materials with relatively high resistivity (ρ ≈ 60–90 Ω·m), likely corresponding to sandy or gravelly materials – permeable but relatively unsaturated. This zone could serve as a favorable area for water infiltration. During intense rainfall events, this water can be released back to the surface by resurgence, particularly in unlined ditches. Moving farther south, the ERT3 profile highlights strong lateral heterogeneity in the terrain under study. Unlike the first two profiles, two main conductive anomalies, trapped within clayey alluvial horizons, were identified in near-perfect alignment with the co-located VLF profile (P2_RN6). These zones are separated by transition zones occupied by moderately resistive formations (ρ ≈ 40–60 Ω·m), which likely correspond to sands or sandy marls with good drainage potential. The deep resistive substrate (ρ ≈ 90 Ω·m) appears at approximately 12 m depth.

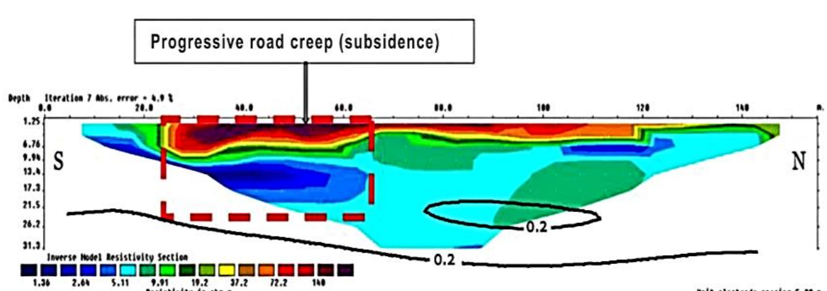

Figure 11. ERT profile My Idriss (Wenner array, S-N direction, 5 m spacing). Black line: DOI = 0.2 threshold.

Figure 12. Aerial view of the RN6–Meknes site illustrating the ERT survey lines.

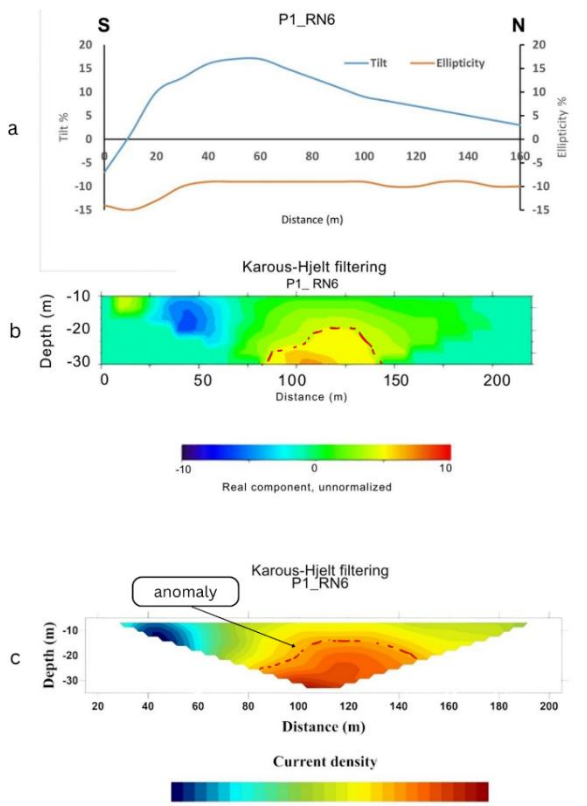

Figure 13. VLF profile RN6 (Meknes) P1: (a) Tilt and Ellipticity, (b) Karous-Hjelt filtering (10 m spacing), (c) Current.

To summarize the results of the ERT profiles, Table 6 groups the main geophysical anomalies by position, depth, resistivity range, and associated geotechnical interpretation.

To characterize the surface horizons, an investigation well S8 (PK 138+500, left bank) was drilled in the roadway. It revealed a bituminous asphalt layer (0–0.15 m), a layer of all-purpose aggregate (0.15–0.50 m), and reddish sand down to 2.10 m. This sequence confirms the presence of reworked and generally coarse materials; it thus provides a useful surface reference point for interpreting the ERT anomalies associated with infiltration.

The spatial extent of the phenomenon and the precise identification of the most sensitive areas allow for targeted corrective measures. These may include installing localized drainage at the anomaly sites, taking measures to limit infiltration (surface improvements and, if necessary, waterproofing), and concreting ditches and road shoulders to sustainably reduce infiltration in this area.

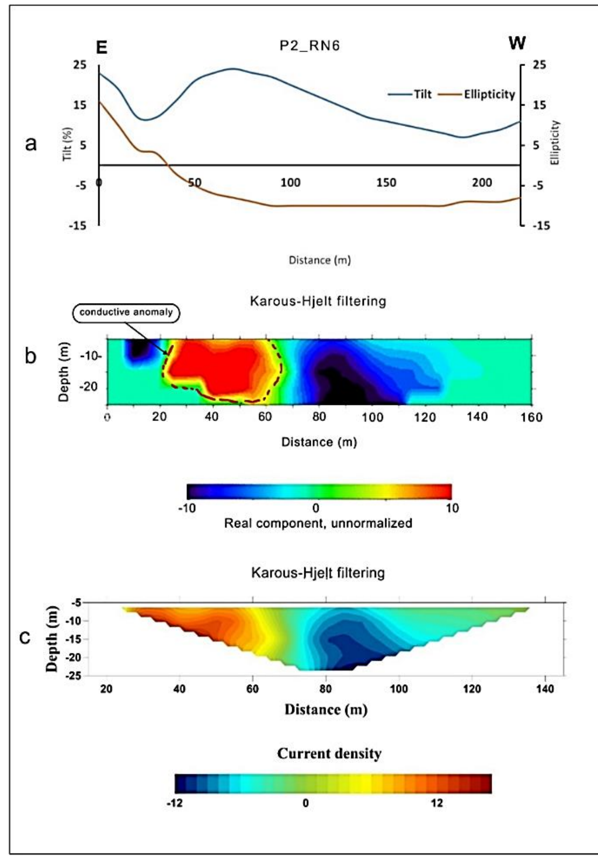

Figure 14. VLF profile RN6 (Meknes) P1: (a) Tilt and Ellipticity, (b) Karous-Hjelt filtering (10 m spacing), (c) Current density.

5. Conclusion

This study evaluated the effectiveness of geophysical methods for diagnosing pavement failures in a marly context. VLF and electrical resistivity tomography were combined for three road sections in the Fes–Meknes region. The two methods are complementary. VLF indicates conductive structures linked to fractures and saturated zones. ERT measures resistivity contrasts and their depth distribution. Consistent VLF anomalies coincide with low-resistivity ERT zones ($\rho <$ 10 Ω·m, with critical values of 2–5 Ω·m at 10–20 m depth), providing considerable confidence in the reliability of this integrated approach.

The results reveal distinct degradation mechanisms at each site. At My Yaacoub, instability appears to be linked to deep fracturing. This is indicated by a major electrical discontinuity between 130 and 160 m along the abandoned road. Surface damage is likely due to saturated marl in the subsoil. At My Idriss, the primary issue is the creep of saturated clays. There is a deep, conductive layer (2–5 Ω·m, 10–20 m) beneath a 6 m-thick road embankment. This reflects a subsidence-reconstruction cycle. The RN6 site (Meknes) is mainly affected by seasonal seepage. This results from preferential infiltration in a more permeable zone (50–90 Ω·m) that supplies the underlying clay horizons.

Pavement defects vary significantly across the three sites. Failures in marly soils result from diverse processes and require tailored technical solutions for each location.

Based on the data, the following solutions are proposed. The route realignment is approved at My Yaacoub. Reinforcement with a geogrid and deep drainage is advised at My Idriss. Targeted drainage, combined with the concreting of hydraulic structures, is recommended on RN6 Meknes.

The non-destructive approach developed provides significant operational benefits. It enables continuous subsurface mapping, optimizes the placement of exploratory boreholes, and reduces the

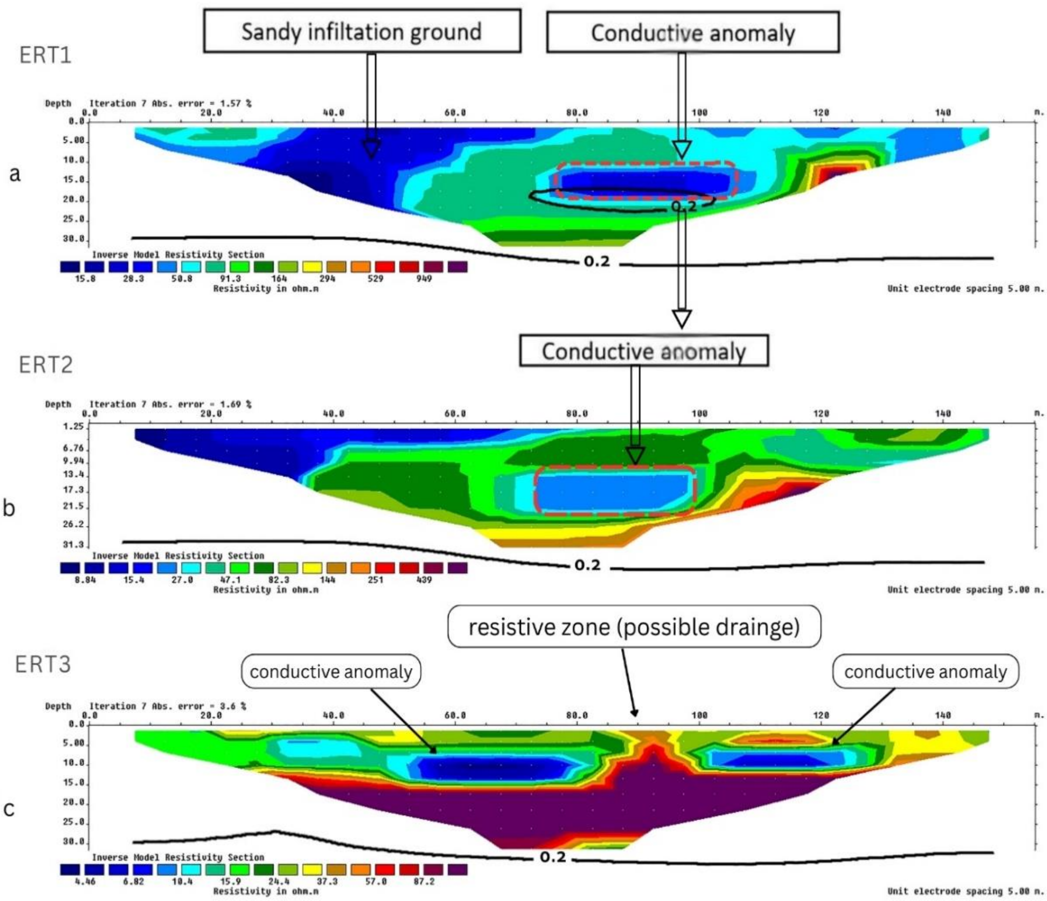

Figure 15. ERT profiles RN6 site (Wenner array, W-E direction): (a) P1, (b) P2 near the plaster factory, (c) P3 located 150 m south. DOI = 0.2 line shown.

number of required boreholes. Its main limitation is the two-dimensional nature of ERT profiles. Future work should include 3D acquisitions and temporal resistivity monitoring. Integration with surface deformation measurement techniques such as InSAR can support more predictive management of road infrastructure in marly areas.

References

[1]. Adenika, C.I., Ariyibi, E.A., Awoyemi, M.O., Adebayo, A.S., Dasho, O.A., & Olagunju, E.O. (2018). Application of geophysical approach to highway pavement failure: a case study from basement complex terrain, southwestern Nigeria. Geo-Engineering, 9, 8. doi: https://doi.org/10.1186/s40703-018-0076-0

[2]. Adesola, A.M., Akinlalu, A.A., & Adelusi, A.O. (2017). Integrated geophysical investigation for pavement failure along a dual carriage way, Southwestern Nigeria: a case study. Kuwait Journal of Science, 44(4), 135–149.

[3]. Akinlalu, A.A., Futai, M.M., Afolabi, D.O., & Abraham-A, R.M. (2026). A review on the application of geophysical methods in civil engineering studies. Geosystems and Geoenvironment, 5(1), 100453. doi: https://doi.org/10.1016/j.geogeo.2025.100453

[4]. Bellanova, J., Calamita, G., Giocoli, A., Luongo, R., Macchiato, M., Perrone, A., Uhlemann, S., & Piscitelli, S. (2018). Electrical resistivity imaging for the characterization of the Montaguto landslide (southern Italy). Engineering Geology, 243, 272–281. doi: https://doi.org/10.1016/j.enggeo.2018.07.014

[5]. Ebrahimi, A., Sundararajan, N., & Ramesh Babu, V. (2019). A comparative study for the source depth estimation of very low frequency electromagnetic (VLF-EM) signals. Journal of Applied Geophysics, 162, 174–185. doi: https://doi.org/10.1016/j.jappgeo.2019.01.007

[6]. Fauchard, C., Antoine, R., Bretar, F., Lacogne, J., Fargier, Y., Maisonnave, C., Guilbert, V., Marjerie, P., Thérain, P.-F., Dupont, J.-P., & Pierrot-Deseilligny, M. (2013). Assessment of an ancient bridge combining geophysical and advanced photogrammetric methods: Application to the Pont De Coq, France. Journal of Applied Geophysics, 98, 100–112. doi: https://doi.org/10.1016/j.jappgeo.2013.07.010

[7]. Forte, E., & Pipan, M. (2017). Review of multi-offset GPR applications: data acquisition, processing and analysis. Signal Processing, 132, 210–220. doi : https://doi.org/10.1016/j.sigpro.2016.04.011

[8]. Hamdi Nasr, I., Issaoui, W., Hallal, N., Lamine, S., Zouaoui, W., Khaskoussi, S., Chaaban, A., Amiri, A., Abidi, O., Hamai, L., & Inoubli, M.H. (2025). Integrated approach for landslide characterization in Northern Tunisia using electrical resistivity tomography, geotechnical analysis, and GIS tools. Geocarto International, 40(1), 2596973. doi: https://doi.org/10.1080/10106049.2025.2596973

[9]. Himi, M., Casas, A., Sendrós, A., Lovera, R., Rivero, L., & Casas-Ponsati, A. (2022). Application of resistivity and seismic refraction tomography for landslide stability assessment in Vallcebre, Spanish Pyrenees. Remote Sensing, 14(24), 6333. doi:

https://doi.org/10.3390/rs14246333

[10]. Karcıoğlu, S., Kaya, M.A., & Gündoğdu, O. (2019). Comparison of the VLF and ERT geo-electrical models on the Avcılar landslide. Yerbilimleri, 40(2), 190–209. doi : https://doi.org/10.17824/yerbilimleri.549104

[11]. Loke, M.H. (2004–2015). Tutorial: 2-D and 3-D Electrical Imaging Surveys. Geotomo Software, Malaysia.

[12]. Maleki, M.R., Uhlemann, S., Piras, D., Farooq, H., Cerfontaine, B., & Merritt, A.J. (2025). Geophysical survey and monitoring of transportation infrastructure slopes (TISs): a review. Geosciences, 15(6), 220. doi: https://doi.org/10.3390/geosciences15060220

[13]. Marescot, L., Loke, M.H., Chapellier, D., Delaloye, R., Lambiel, C., & Reynard, E. (2003). Assessing reliability of 2D resistivity imaging in mountain permafrost studies using the depth of investigation index method. Near Surface Geophysics, 1, 57–67. doi: https://doi.org/10.3997/1873-0604.2002007

[14]. Oguntade, O., Olorunfemi, M.O., & Ajayi, E.O. (2022). Subsurface investigation for road construction using electrical resistivity method along Oloko Road, Nigeria. Annals of Science and Technology, 7(1), 29–35. doi: https://doi.org/10.2478/ast-2022-0004

[15]. Olayanju, G.M., Mogaji, K.A., Lim, H.S., & Ojo, T.S. (2017). Foundation integrity assessment using integrated geophysical and geotechnical techniques: case study in crystalline basement complex, southwestern Nigeria. Journal of Geophysics and Engineering, 14(3), 675–690. doi: https://doi.org/10.1088/1742-2140/aa64f7

[16]. Oldenburg, D.W., & Li, Y. (1999). Estimating depth of investigation in dc resistivity and IP surveys. Geophysics, 64(2), 403–416. doi : https://doi.org/10.1190/1.1444545

[17]. Perrone, A., Lapenna, V., & Piscitelli, S. (2014). Electrical resistivity tomography technique for landslide investigation: a review. Earth-Science Reviews, 135, 65–82. doi: https://doi.org/10.1016/j.earscirev.2014.04.002

[18]. Reynolds, J.M. (2011). An Introduction to Applied and Environmental Geophysics (2nd Ed.). Wiley-Blackwell, Chichester, UK.

[19]. Saad, A.M., Sabet, H.S., Ismail, A.M., El-Ashaal, A., & Kamal, H.M. (2024). Geotechnical and geophysical investigations for infrastructure safety zones: a case study of the supporting ring road, Cairo, Egypt. Scientific Reports, 14, 29670. doi : https://doi.org/10.1038/s41598-024-72337-8

[20]. Sun, X., Chen, X., Huang, Y., Zhou, J., Liang, Y., & Wang, L. (2024). Electrical Resistivity Tomography (ERT) investigation for landslides: case study in Hunan Province, China. Applied Sciences, 14(7), 3007.doi: https://doi.org/10.3390/app14073007

[21]. Tsai, W.-N., Huang, P.-T., Chiang, S.-H., Huang, Y.-T., & Hsiao, Y.-S. (2021). Electrical Resistivity Tomography (ERT) monitoring for landslides: case study in the Lantai area, Yilan Taiping Mountain, Northeast Taiwan. Frontiers in Earth Science, 9, 737271. doi: https://doi.org/10.3389/feart.2021.737271

[22]. Uhlemann, S., Hagedorn, S., Dashwood, B., Maurer, H., Gunn, D., Dijkstra, T., & Chambers, J. (2016). Landslide characterization using P- and S-wave seismic refraction tomography — The importance of elastic moduli. Journal of Applied Geophysics, 134, 64–76. doi: https://doi.org/10.1016/j.jappgeo.2016.08.014

[23]. Barker, R.D. (1989). Depth of investigation of collinear symmetrical four-electrode arrays. Geophysics, 54(8), 1031–1037. doi: https://doi.org/10.1190/1.1442728

[24]. Robert, T., Dassargues, A., Brouyère, S., Kaufmann, O., Hallet, V., & Nguyen, F. (2011). Assessing the contribution of electrical resistivity tomography (ERT) and self-potential (SP) methods for a water well drilling program in fractured/karstified limestones. Journal of Applied Geophysics, 75(1), 42–53.doi: https://doi.org/10.1016/j.jappgeo.2011.06.008

[25]. Marescot, L., & Loke, M.H. (2003). Application de l'indice DOI à l'imagerie électrique 2D pour les sous-sols à forts contrastes de résistivité. Technical paper (4 pp.).

[26]. Loke, M.H. (2002). RES2DINV: Rapid 2-D Resistivity and IP inversion using the least-squares method. Geotomo Software, Penang, Malaysia.

[27]. Benmakhlouf, M. (2001). Les sources thermales du Maroc septentrional : relation entre le thermalisme et la tectonique. Thèse de doctorat, Université Mohammed V, Rabat, Maroc.